Bulletin of the Seismological Society of America, Vol. 86, No. 5, pp. 1255–1269, October 1996

Toward Real-Time Estimation of Regional Moment Tensors

by Michael E. Pasyanos, Douglas S. Dreger, and Barbara Romanowicz

Abstract Recent advances in broadband station coverage, continuous telemetry systems, moment-tensor procedures, and computer data-processing methods have given us the opportunity to automate the two regional moment-tensor methods employed at the UC Berkeley Seismographic Station for events in northern and central California. Preliminary solutions are available within minutes after an event has occurred and are subsequently human reviewed. We compare the solutions of the two methods to each other, as well as the automatic and revised solutions of each individual method. Efforts are being made to establish robust criteria for determining accurate solutions with human review and to fully automate the moment-tensor procedures into the already-existing automated earthquake-location system.

Introduction

The installation of continuously telemetered, digital, high-dynamic range, broadband instruments of the Berkeley Digital Seismic Network (BDSN) (Romanowicz *et al.,* 1992, 1994) has made it possible to perform regional moment-tensor calculations for moderate-sized earthquakes in and around the network area. In fact, two different regional moment-tensor procedures were developed to calculate source parameters: a frequency-domain surface-wave method and a time-domain complete waveform method (Romanowicz *et al.,* 1993). At the same time, the Rapid Earthquake Data Integration (REDI) system was developed to rapidly respond to earthquakes (Gee *et al.,* 1996). This system automatically locates, determines the magnitude, and issues notifications of earthquakes in California.

Recently, efforts have been made to produce reliable focal mechanisms in as timely a manner as possible. This is to rapidly determine the faulting style of the events and to estimate the seismic moment. Characterization of the fault orientation is important for rapid hazard analysis because aftershock production differs among fault types (Uhrhammer, 1986), and fault orientation is important for preliminary estimates of directivity. In addition, recently, King *et al.* (1994) have shown that regional static stress changes induced by mainshocks can lead to identification of likely areas of increased aftershock activity. To accomplish the goal of rapid fault-plane estimation, the moment-tensor methods were streamlined, the velocity models were accurately calibrated, and the procedures began to make use of the rapid locations of the already-existing REDI system. Since June 1994, the procedures for determining regional moment tensors for northern and central California have been fully automated. As a result, a preliminary computer-determined solution is available within 9 to 15 min after the occurrence of an event. The solutions are currently reviewed by an analyst, and the information is disseminated to the outside community via E-mail messages (see Appendix). In this article, we evaluate the possibility of releasing regional moment-tensor information automatically. In the near future, these automatic moment-tensor procedures will be fully integrated into the REDI processing.

The basic data for the inversions are recorded by the broadband BDSN network. These are three-component, digital, high-dynamic range, very broadband velocity transducers. Collocated at each site are FBA-23 accelerometers. Both data streams are digitized at various rates on 24-bit Quanterra data loggers. The combined system gives a nominal dynamic range of 200 dB, which is essential for being able to monitor the full range of earthquake sizes occurring in California. Figure 1 shows the distribution of stations across northern and central California. The data have been telemetered back to Berkeley via a variety of media such as digital ADN phone lines, microwave, and radio circuits and are available for retrieval within about 30 sec after recording in the case of VBB data and within about 7 min in the case of LP data. Currently, most BDSN station telemetry uses 56-kbit frame relay protocols on digital phone services. The data is then archived on an optical mass-storage "jukebox" in a compressed file format. Both moment-tensor procedures are activated using the UNIX *cron* command, which causes the system to wake up every few minutes to see if any new events have arrived. At this point, the two procedures are processed independently and will be considered separately.

Regional Surface-Wave Inversion

In the regional surface-wave inversion method, the first of two methods that we consider here, we invert intermediate-period Love and Rayleigh waves that are recorded regionally, using a two-step inversion procedure originally designed for global applications (Romanowicz, 1982;

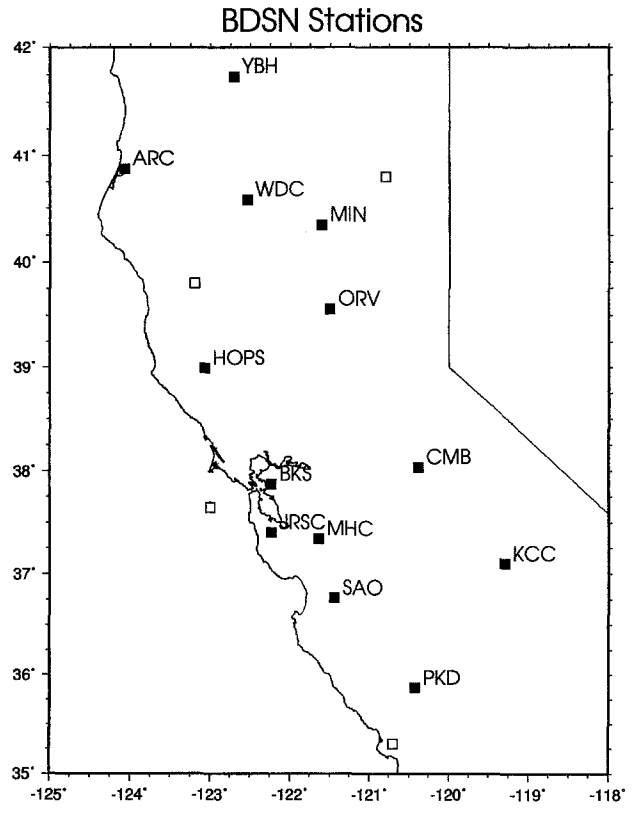

Figure 1. Broadband stations in the Berkeley Digital Seismic Network (BDSN). Stations operational as of February 1996 are shown by filled squares. Planned stations are shown by empty squares.

Romanowicz and Monfret, 1986) and adapted to the regional case (Patton and Zandt, 1991; Romanowicz *et al.*, 1993). Generally, the procedures are robust and work well if the following conditions are met: (1) there is a reasonably good hypocentral location, (2) the source-receiver structure is accurately calibrated, and (3) noisy stations are removed. Since this is not always the case, we will discuss the biases that might be caused by nonideal conditions. If the preliminary information indicates that the event is large enough to process using the regional surface-wave method, then a working directory is created for the event. Even though the current minimum magnitude earthquakes we can process using this method is about M 3.6, we start processing events with $M \geqq 3.4$ in order to account for variations in magnitude determination.

Data are extracted from the Northern California Earthquake Data Center (NCEDC) and rotated from a station reference frame (Z,N,E) into an earthquake reference frame (Z,R,T). The computer-determined epicentral locations are assumed as the centroid location. Small errors in the epicenter will not be significant, but large errors can affect the rotation into the earthquake reference frame, as well as the assumed station-receiver distance. Small errors in the origin time are effectively absorbed by changes in the estimated source duration. Because this procedure is a frequency-domain method, the data are then transformed to the spectral domain using a fast Fourier transform. Depending on the size of the event, different periods are selected for the moment-tensor inversion. In practice, for moderate-sized events ($M < 5.5$), a range of periods are chosen between 15 and 45 sec, and larger events ($M \geqq 5.5$), from 25 to 70 sec.

At this point, an appropriate model is selected for each source-receiver path, in order to account for lateral heterogeneity. This is accomplished by applying a phase velocity correction appropriate for one of five calibrated regional models. The existing regional models are Coast Ranges, Great Valley, Sierra Nevada, southern California, and Basin and Range Province. Not properly accounting for the structure at this point can introduce noise into the procedure. Improvements in the future include dropping the regionalization scheme and dynamically determining the appropriate structure along each source-receiver path from a three-dimensional model of phase velocity.

Finally, the stations are selected, and the inversion is performed. For the automated procedures, it is important to be able to choose only those stations that will have a high signal-to-noise ratio. This is accomplished (in the surface-wave procedure) by assigning to each station and component a parameter based on the long-term noise characteristics of each station. We have found that an effective way of characterizing the overall noise level is to calculate the power spectral density of noise windows for each station and component. Taken daily over a long time period, such as a year, we can determine the typical levels of the microseismic noise at that station. For example, over a one-year period from July 1994 to July 1995, the low-frequency (32 to 128 period) power spectral density at station YBH was -172 ± 2 dB and -169 ± 2 dB for the vertical and horizontal components, respectively, classifying them both as quiet components. In general, we find hard-rock sites located away from the coastline to be our quietest stations. Stations located on less-competent rock or close to shore tend to be noisier. Unsurprisingly, the noise is higher on the horizontal components than on the vertical components. This noise parameter, as well as the preliminary magnitude and source-receiver distance, is used to determine whether or not this particular component should be used in the moment-tensor inversion.

Using the selected stations, the two-step frequency-domain surface-wave inversion is performed (Romanowicz and Monfret, 1986) for a range of trial centroid depths. Figure 2 illustrates an example of the regional surface-wave method for an earthquake located near Hollister, California, on 16 June 1995. The automated solution (shown with dotted lines) was very close to the revised estimation of source parameters (shown in solid lines), differing primarily in the estimation of source depth. The automated moment-tensor solution was available about 5 min after the epicentral information was received and about 10 min after the event occurred.

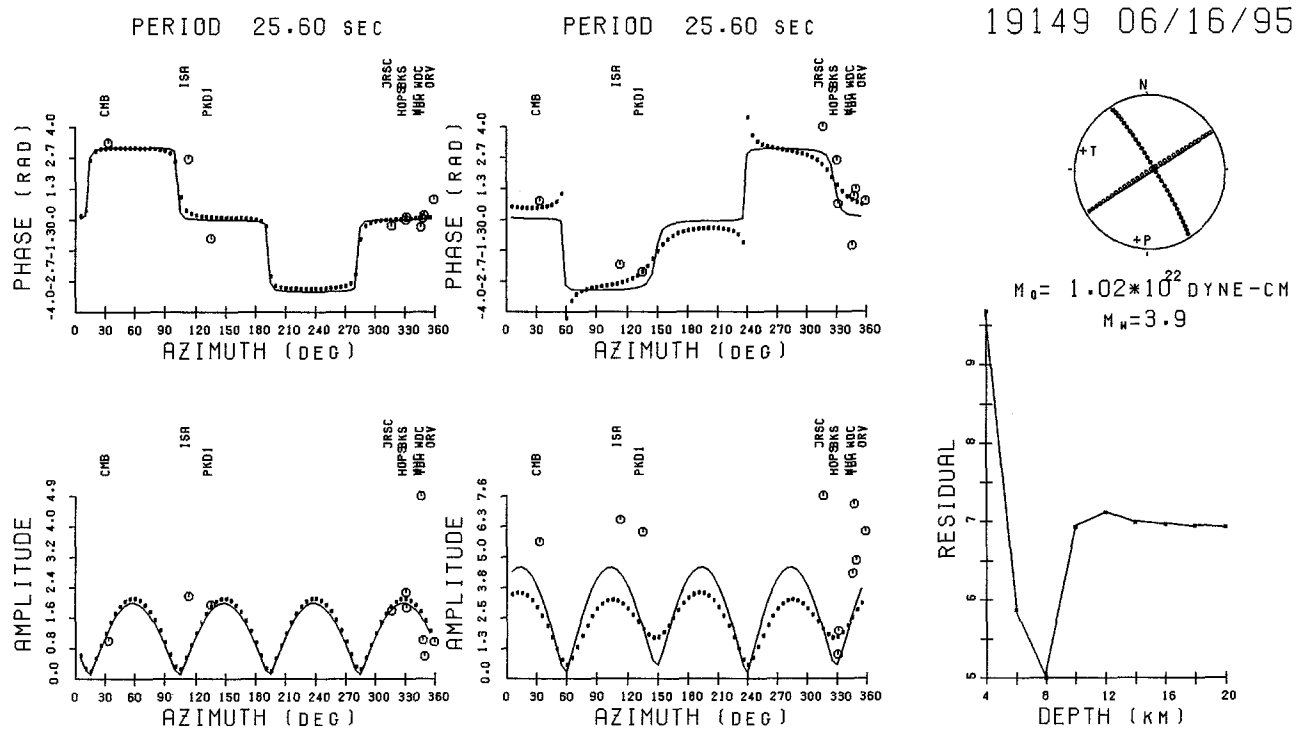

INITIAL	FINAL		
Mo = 1.5e22 dyne-cm	Mo = 1.0e22 dyne-cm	21:20:36	Event origin time
Mw = 4.08	Mw = 3.97	21:27	REDI Page
NP1 238/88/-6	NP1 58/89/6	21:29	Data Extracted
NP2 328/84/-178	NP2 328/84/179	21:31	Inversion Completed
z = 20 km	z = 8 km	21:32:14	MT Page is sent
tau = 1.0 sec	tau = 1.0 sec		

Figure 2. Example of the regional surface-wave method for an event located near Hollister, California, on 16 July 1995. (a) Automatic (small circles) and revised (solid lines) amplitude and phase fits to the data (large circles) for Love waves at 25.6-sec period. (b) Same as for (a) for Rayleigh waves. (c) Focal mechanism of automatic and revised mechanisms and residual versus depth curve for the revised inversion. The source parameters of the initial and final solutions (M_0, M_w, nodal planes 1 and 2, centroid depth, and half-duration), along with relevant time information, are indicated at the bottom of figure.

Time-Domain Moment-Tensor Estimation

The time-domain moment-tensor procedure is activated in the same manner as the surface-wave approach. Currently, the minimum magnitude that is processed is set at M 3.5. This value reflects the limits imposed by the background noise in the frequency passband used by the inversion. Three passbands are employed: 50 to 10 sec ($3.5 \leqq M < 4.0$), 50 to 20 sec ($4.0 < M < 5.0$), and 100 to 20 sec ($M \geqq 5.0$). Two velocity models are used. These models were determined by forward modeling broadband data for various paths throughout California (e.g., Dreger and Helmberger, 1993; Dreger and Romanowicz, 1994). The long-period waves that are used are relatively insensitive to the details of crustal structure; however, the two models that are employed are representative of the gross changes in crustal thickness, average crustal velocity, and near-surface velocity gradient. To obtain the desired reduction in moment-tensor processing time, the theoretical Green's functions computed using these models are stored on-line. These Green's functions are prefiltered using the three passbands described above.

The inverse procedure itself makes several assumptions. First, it is constrained to only the deviatoric tensor, neglecting volumetric changes of the source. Second, a point source in both space and time is assumed. Source depth is found by iteration and evaluating an objective function that depends upon both the RMS of the difference between the data (d) and the synthetic waveforms (s), modulated by the percent double couple (pdc):

$$\text{fit} = \frac{\text{RMS}(d - s)}{\text{pdc}}. \qquad (1)$$

Smaller numbers indicating better fits are obtained when both the waveform misfit $(d - s)$ is small and the pdc is large. Another measure that is used is the variance reduction:

$$1.0 - \frac{\int [d - s]^2 \, dt}{\int d^2 \, dt}, \qquad (2)$$

where d is the data and s is the synthetic.

The current procedure utilizes the three closest stations in the distance range from 50 to 400 km. This ensures reasonably good azimuthal coverage. Although three-component waveform inversion of a single station may resolve the moment-tensor parameters (Dreger and Helmberger, 1991), the use of multiple stations improves the stability of the results. Figure 3 illustrates the three-component time-domain inverse approach for the same event as shown in Figure 2. Figure 3a shows the automated result. In this particular case, the 50- to 20-sec passband was used. The revised solution, which was released via E-mail, was obtained by searching the depth parameter space (depth remained at 11 km) and adding station CMB to provide better azimuthal coverage, particularly by adding P_{nl} and Rayleigh waves to the inversion. Clearly, the automated and revised solutions are nearly the same, and in this particular case, processing was completed 9 min after the origin time. The automated solutions are not always correct, as discussed in the following section, and the calibration of the system is a continuing effort.

The procedure we employ differs from other CMT-type inversions (Dziewonski *et al.*, 1981; Ritsema and Lay, 1993) in that only the high-frequency location is used, the data are not aligned according to the event origin time, and a revised centroid location is not solved for. Rather, the Green's functions are optimally aligned to the data using a cross-correlation function. This level of approximation affords a greater level of flexibility in rapid source-parameter determinations when event locations and origin time are preliminary. It has been shown through sensitivity analysis that event mislocations on the order of 15 km can be tolerated by this procedure (Dreger and Helmberger, 1993), and in practice, these assumptions have been found to be reasonable for events in the magnitude range from 3.5 to 7.3.

Moment-Tensor Comparisons

It has already been successfully demonstrated that the two regional moment-tensor methods produce similar results

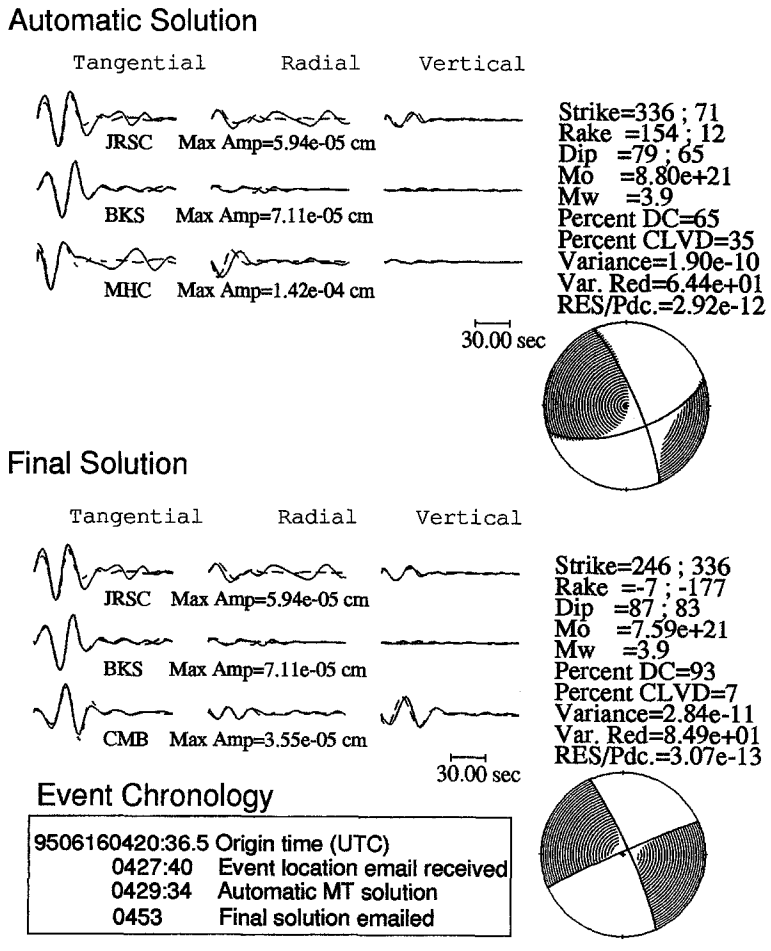

Figure 3. Compares the automated and revised solutions for the same M_w 3.9 event discussed in Figure 2. The initial solution included stations BKS (143 km), JRSC (100 km), and MHC (68 km). The revised solution was E-mailed after the addition of the CMB station (172 km). The complete waveforms include P_{nl}, S_n, Love, and Rayleigh waves.

(Figs. 2 and 3 for earthquakes over a large magnitude range (Romanowicz *et al.*, 1993). Based on comparing the mechanisms, we find that differences in the angles of the focal mechanism of about 10° and differences in the seismic scalar moment of about 50% can be expected (Ritsema *et al.*, 1994; Dreger *et al.*, 1995). Sources of noise include ambient noise levels, source complexity for large events and oversimplification of crustal structure models. The latter is likely to be the most important, and, therefore, we use the two methods outlined in this article to help ascertain the implications of the necessary oversimplification of crustal models. Studying the remaining differences is important in quantifying changes that might be needed to the existing methods, in calibrating structure, for example. At this point, we need an objective function to measure the differences between any two given moment tensors. This function is useful in comparisons between moment-tensor solutions obtained using different methods and in comparisons between automatic and revised solutions. We also require this function to be dependent strictly on mechanism, and not on the seismic scalar moment, which can be compared separately.

We define the moment-tensor difference function μ as the root mean square of the differences of the nine moment-tensor elements normalized by their respective seismic scalar moment M_0.

$$\mu = \sqrt{\frac{\sum_{i=1}^{3}\sum_{j=1}^{3}(M_{ij}^{(1)\prime} - M_{ij}^{(2)\prime})^2}{8}} = \sqrt{\frac{\sum_{i=1}^{3}\sum_{j=1}^{3}(\delta M_{ij}')^2}{8}}, \quad (3)$$

where $M_{ij}' = M_{ij}/M_0$. The $\sqrt{8}$ normalization factor causes μ to range from a value of 0 (for a perfect fit) to a value of 1 (for double-couple mechanisms of exactly the opposite sense of motion). In this manner, we are able to objectively measure the difference in the estimated source mechanisms. Figure 4 illustrates μ as a function of mechanism change. The first and second columns show the change due to a rotation in strike and dip on a strike-slip mechanism. The third column shows the effect of a change in rake for a reverse mechanism, and the last column shows the change of a rotation in strike on a normal mechanism. For values of $\mu < 0.25$, the focal mechanisms are essentially the same but start to diverge for $0.25 < \mu < 0.50$. For $\mu > 0.50$, the mechanisms are significantly different from one another.

First, we consider the comparison between the two methods for moment magnitude M_w. In all cases, our comparisons consider all events determined by the two methods for the 3½-yr time period from January 1991 to June 1995. Figure 5 shows M_w obtained from the regional surface-wave method plotted against those obtained from the regional waveform method for 63 events. In general, they compare very well. The least-squares fit to the data indicates that there is a slight bias toward a higher magnitude for the surface-wave method as compared to the waveform method. A sta-

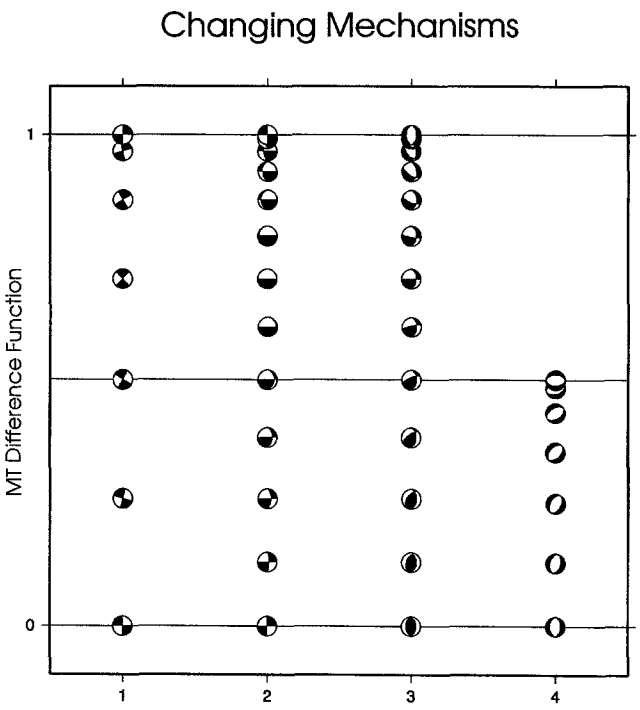

Figure 4. Variations in the moment-tensor difference function μ for changes in strike, rake, and dip angles. The first column shows a change in strike, the second column shows a change in dip, the third column shows a change in rake, and the last column shows a change in rotation for a normal mechanism. Mechanism 1 is fixed, as shown on the bottom line; mechanism 2 is perturbed, as shown in each column.

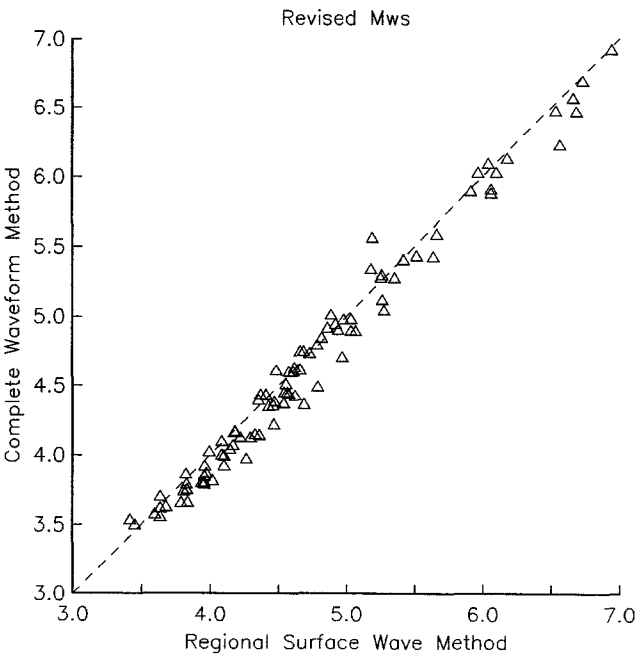

Figure 5. A comparison of the M_w's for revised events from the regional surface-wave and complete waveform methods for all events in the catalog.

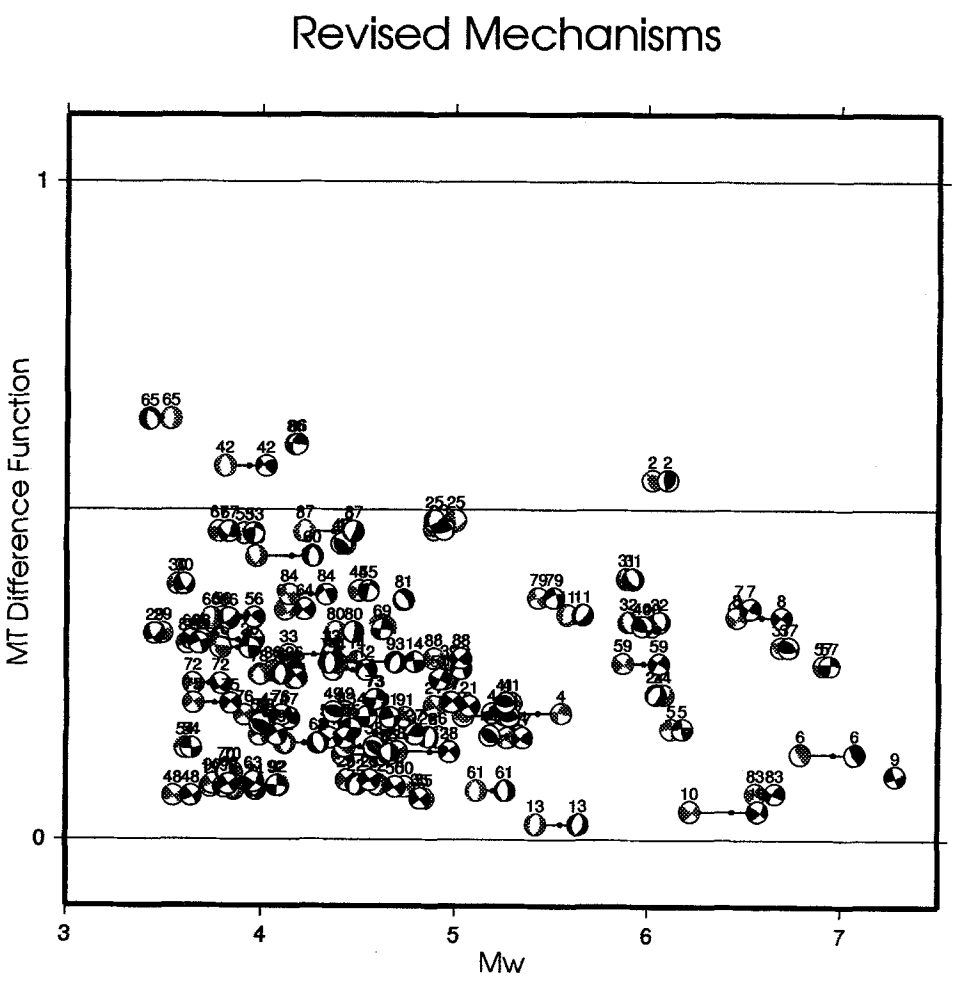

Figure 6. A comparison of the revised regional surface-wave (black) and complete waveform (gray) moment-tensor solutions for all events from January 1991 to July 1995. Numbers above the focal mechanisms are listed in chronological order. The x axis is moment magnitude M_0, the y axis is the moment-tensor difference function μ.

tistical comparison of the differences shows that the mean difference is 0.075, and the standard deviation of the difference is 0.011. These values are several times better than comparisons between other magnitudes (M_w versus M_L, M_w versus M_d, M_L versus M_d) that are compared later in the article. There is therefore less bias and less scatter in the use of M_w as an estimation of earthquake size. In a few rare cases in The Geysers (8/23/93 and 8/29/94), the moment-magnitude determinations are between a half to a full magnitude unit higher than the other determinations (M_L and M_d) but consistent with each other, indicating a larger earthquake source whose high-frequency energy is being attenuated significantly near the source. This seems to confirm that moment magnitude, even regionally determined, is the most robust determination of magnitude.

Even so, there seems to exist a slight bias between the two moment determinations that is significant in light of the typical variations. One possible explanation is that differences in the models used by the individual inversion methods, particularly the attenuation quality factor Q, are causing the discrepancy. Unfortunately, this simple explanation does not seem to bear out. Tests of the moment-tensor inversion using a wide range of Q values show that attenuation is a highly insensitive parameter. Changes in Q_s ranging from 200 to 950 have little or no effect on either the mechanism or the seismic scalar moment. The reason is that the periods used in the moment-tensor inversion (>15 sec) have such large wavelengths that the number of cycles over the typical distance ranges (in this case, 100 to 600 km) used are small.

Other tests using synthetic data show that both methods recover the same mechanisms and scalar moments. This rules out the possibility that there are inherent differences in the two different regional methodologies. A more likely explanation is that the differences are caused by the imperfect estimation of the velocity structure of the earth. Dreger and Helmberger (1993) have compared various models and have found that changes in velocity model parameters, such as the average crustal velocity, can have large effects on the inversion. The refined calibration of the velocity structure of the earth is an ongoing effort that should improve with time

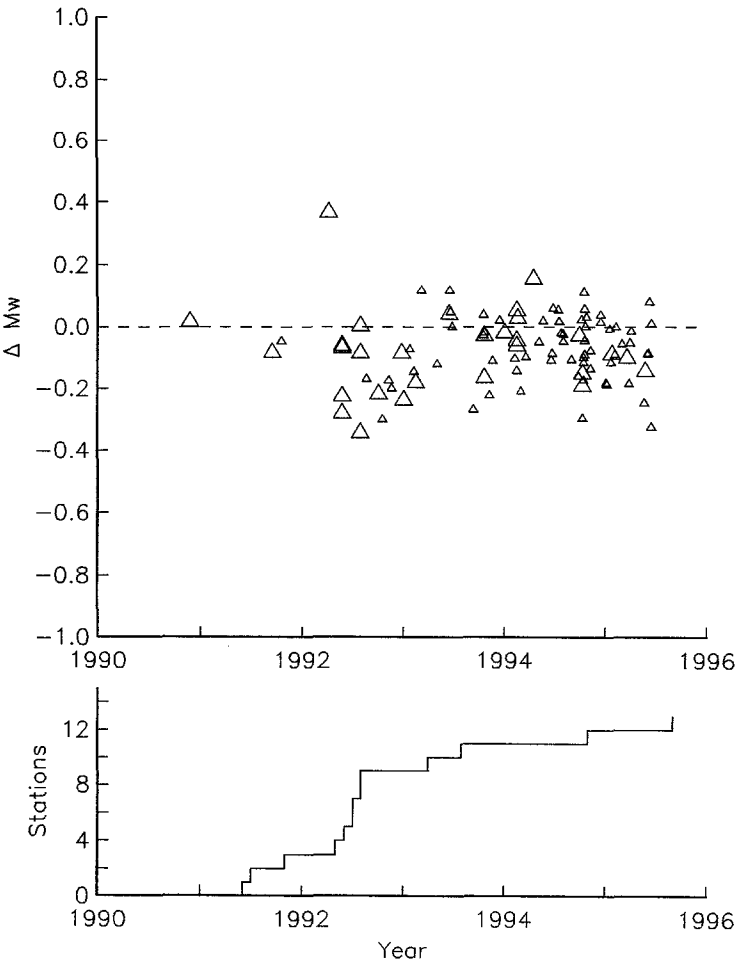

Figure 7. Moment tensors versus time: (a) shows differences in M_w between the two methods as a function of time; (b) illustrates the number of broadband stations in operation as a function of time. Events greater than magnitude 5.0 are shown by larger symbols.

and by continuing to compare earthquake solutions from the two regional methods.

Next, we use the function μ to compare the mechanisms to each other. Figure 6 shows the "beachballs" of the mechanism plotted at the location of μ and the individual $M'_w s$. Most of the events plot below the $\mu = 0.5$ cutoff which, as mentioned earlier, indicates that the solutions are similar. There are a few exceptions, most of which either are close to the M 3.5 cutoff for the regional methods or were determined early in the development of the codes, at a time when BDSN had relatively few operational stations. It should also be noted that the moment-tensor methods have evolved with time. In addition to the continued refinement of the velocity models, early on, the broadband station coverage was sparse and distant, and noisier stations were more strongly depended upon. The evolution of moment tensors with time, along with the number of broadband stations in BDSN, is illustrated in Figure 7. Over time, the number of events calculated has increased dramatically. Although the largest discrepancies in moment magnitude do not appear to change much with time, we are seeing very consistent moment magnitudes for the largest events, and the largest discrepancies occur for the smaller events that are approaching the noise floor.

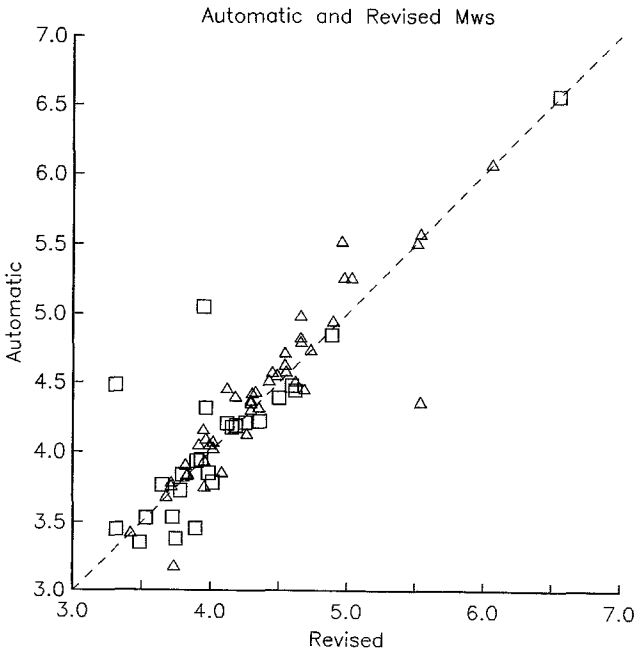

Figure 8. A comparison of the automatic and revised M_w's for all events in the catalog. Triangles are values from regional surface-wave method. Squares are those from the complete waveform method.

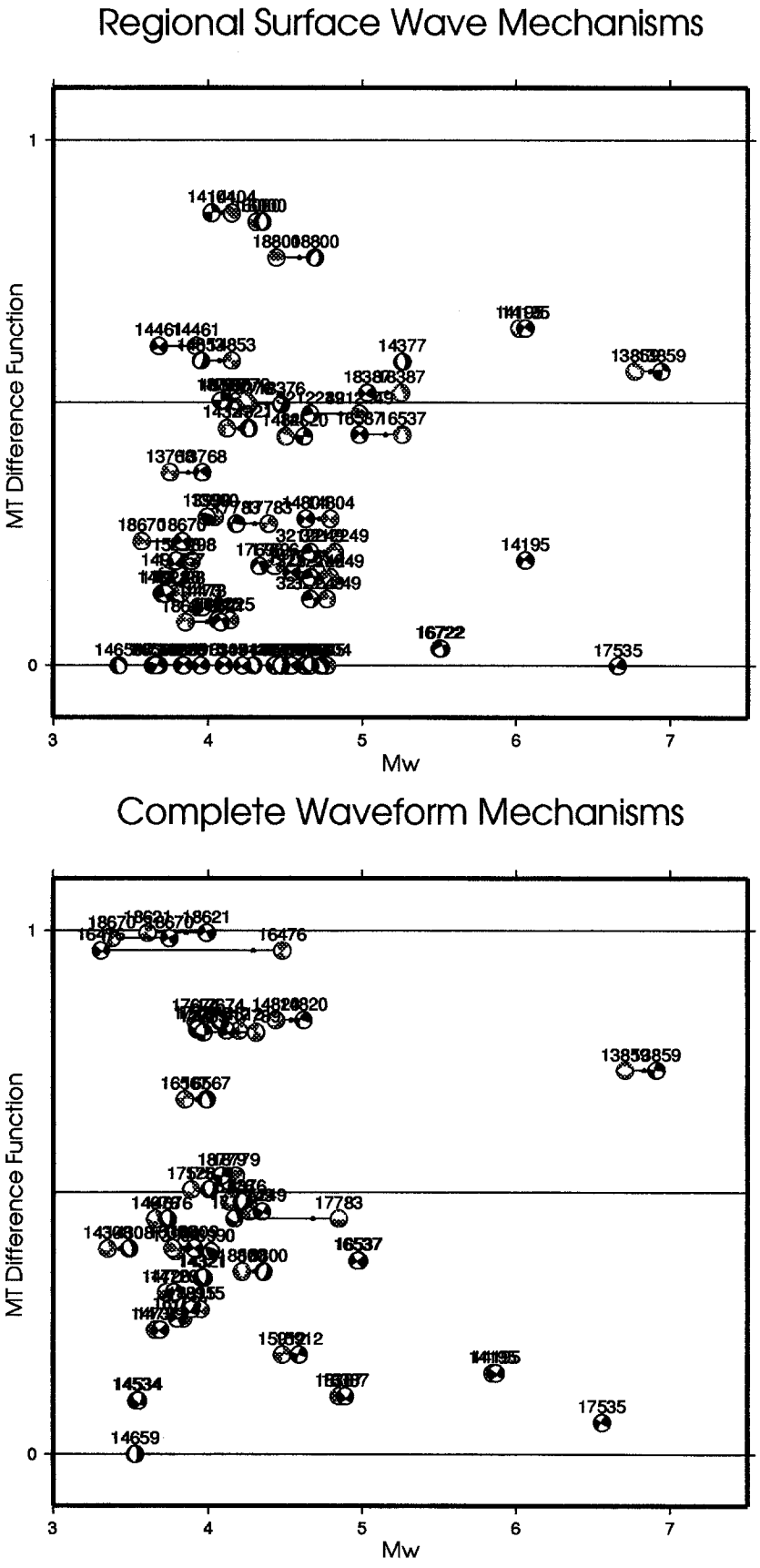

Figure 9. A comparison of the automatic (gray) and revised (black) moment-tensor solutions for both regional surface-wave and complete waveform methods. Axes are the same as those in Figure 6. Numbers above the focal mechanisms are REDI event numbers.

Since our goal is to determine moment tensors automatically and to distribute this preliminary information to outside agencies without human intervention, we compare the automatic mechanisms to the revised, human-reviewed mechanisms. Figure 8 shows a plot similar to Figure 5 comparing the M_w of the automatic solutions from both regional methods to the revised solutions. Again, M_w appears to be a relatively robust parameter and, even for solutions with incorrect determinations of mechanism and/or depth, M_w does not usually vary by more than 0.2. The corresponding plot for mechanisms is shown in Figure 9. Obviously, there are more significantly different mechanisms in this comparison than in the comparison of the two revised solutions. In 78% (38/49 cases) of the surface-wave moment tensors and 61% (19/31 cases) of the complete waveform moment tensors, the mechanisms plot below the $\mu = 0.5$ cutoff, indicating a reasonable solution. In a substantial number of cases, the automatic solution was very good, and little or no further revisions were made. Event 13859, an event off the coast of Mendocino, is an obvious outlier in both cases. Generally, however, it appears that the automated solutions are behaving relatively well.

Can we devise a procedure to check the preliminary solutions to determine their accuracy? One possible method

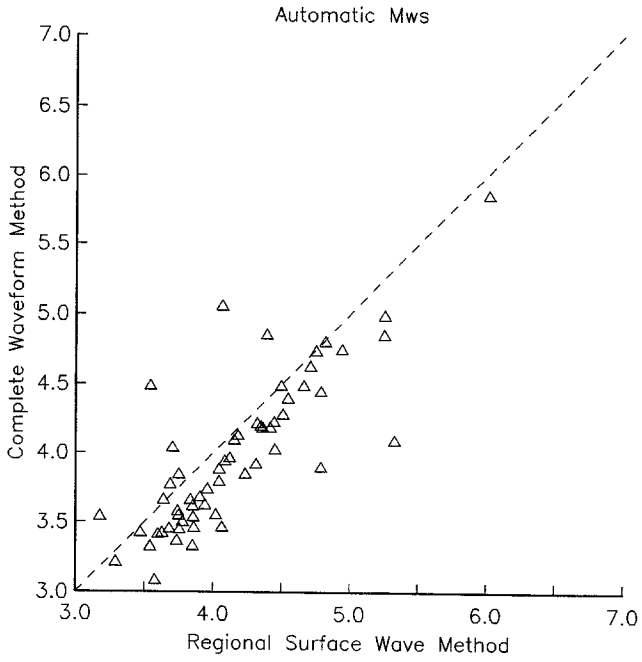

Figure 10. A comparison of the automatic M_w's for all true events in the catalog. Splits and microwave glitches have been removed.

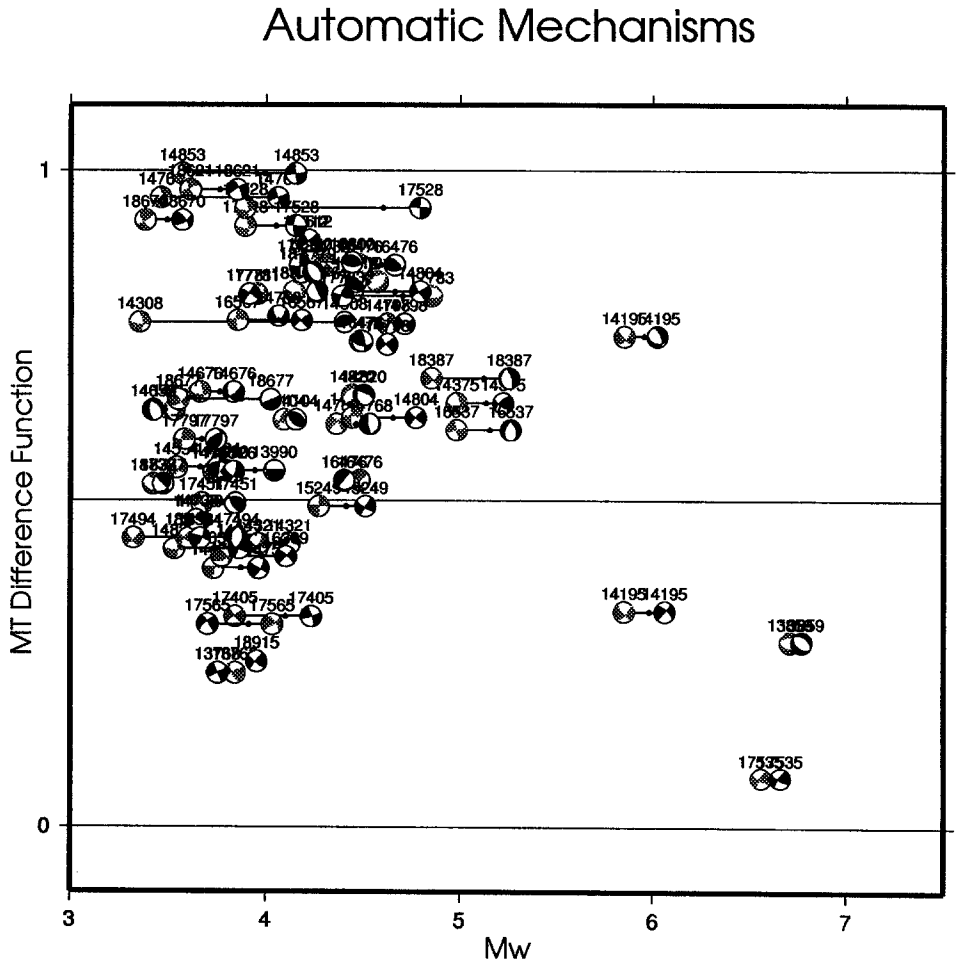

Figure 11. A comparison of the automatic regional surface-wave (gray) and complete waveform (black) moment-tensor solutions. Axes are the same as those in Figure 6. Numbers above the focal mechanisms are the REDI event numbers.

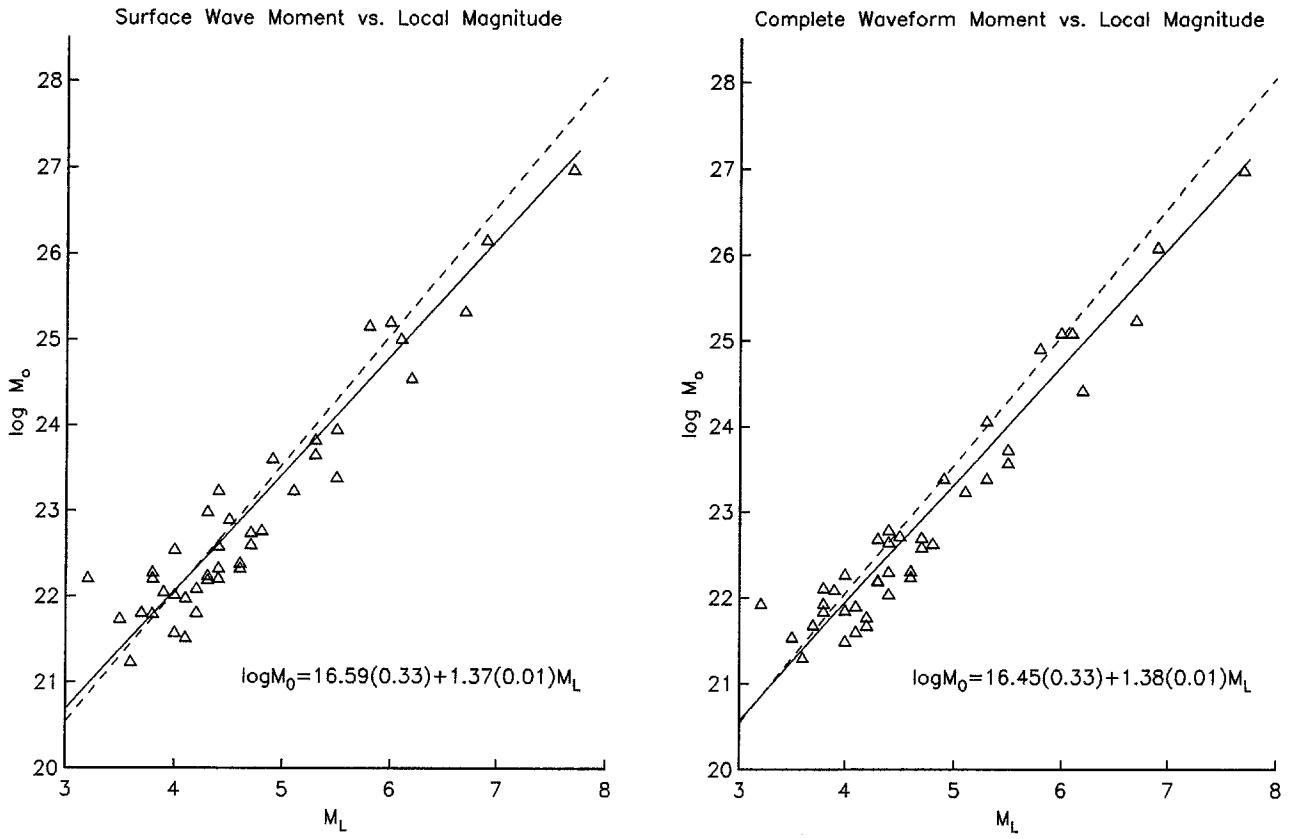

Figure 12. A comparison of M_0 and M_L for all events in the catalog. The solid line shows the least-squares fit to the data. (a) Comparison for surface-wave method and (b) comparison for complete waveform method.

is by comparing the two automatic mechanisms. In cases where the automatic mechanisms agree, we have in general a robust estimator of the source mechanism. Figures 10 and 11 show a comparison between the automatic moment-tensor methods. Because the automatic events would include all cases where the automatic moment tensors have been initiated, including microwave glitches, "splits" of real events, events at the moment-tensor threshold, or anything that is initially determined by the real-time system to be an event, the figures have been culled to only include those events that eventually were human-reviewed and processed completely. In this case, we only have 31% (11/35 cases) of the events plotting below the $\mu = 0.5$ cutoff. The three largest events show very good agreement. Unfortunately, event 13859 had poor mechanisms that were similar between the two methods. For the other two M_w 5 events (16537 and 18387), the automatic solutions were dissimilar, but the mechanism of one of the methods was good.

Comparison with Other Magnitudes

Next, we show how the values of M_0 compare to those of local magnitude M_L and coda duration magnitude M_d (Figs. 12 and 13). Although the scatter that we see in the two figures is about the same, the values that we get by fitting a least-squares line of the form $\log(M_0) = a + bM$ is much more consistent for the M_0/M_d comparison. The best-fitting lines are $\log(M_0) = 16.59 + 1.37M_L$, $\log(M_0) = 16.45 + 1.38M_L$, $\log(M_0) = 16.26 + 1.51M_d$, and $\log(M_0) = 16.14 + 1.51M_d$ for the surface-wave and complete waveform measurements, respectively. Moment magnitude has been defined where $a = 16.1$ and $b = 1.5$ (Thatcher and Hanks, 1973; Hanks and Kanamori, 1979). In light of these numbers, the comparisons of scalar moment to duration magnitude are particularly good, with slightly lower estimates of duration magnitude than the moment magnitudes, but stable over a wide magnitude range. Comparisons to local magnitude, however, show that the local magnitude is consistently higher, with particularly large discrepancies at higher magnitude levels. These results indicate that the relationship between M_0 and magnitude originally determined, and more recently tested for regional moment tensors in Southern California (Thio and Kanamori, 1995), also holds for earthquakes in Northern California.

A statistical comparison for all of the events considered, irrespective of magnitude, is shown in Table 1. We find that the overall differences between M_w and M_L are -0.053 ± 0.096 and -0.128 ± 0.079 for the surface-wave and com-

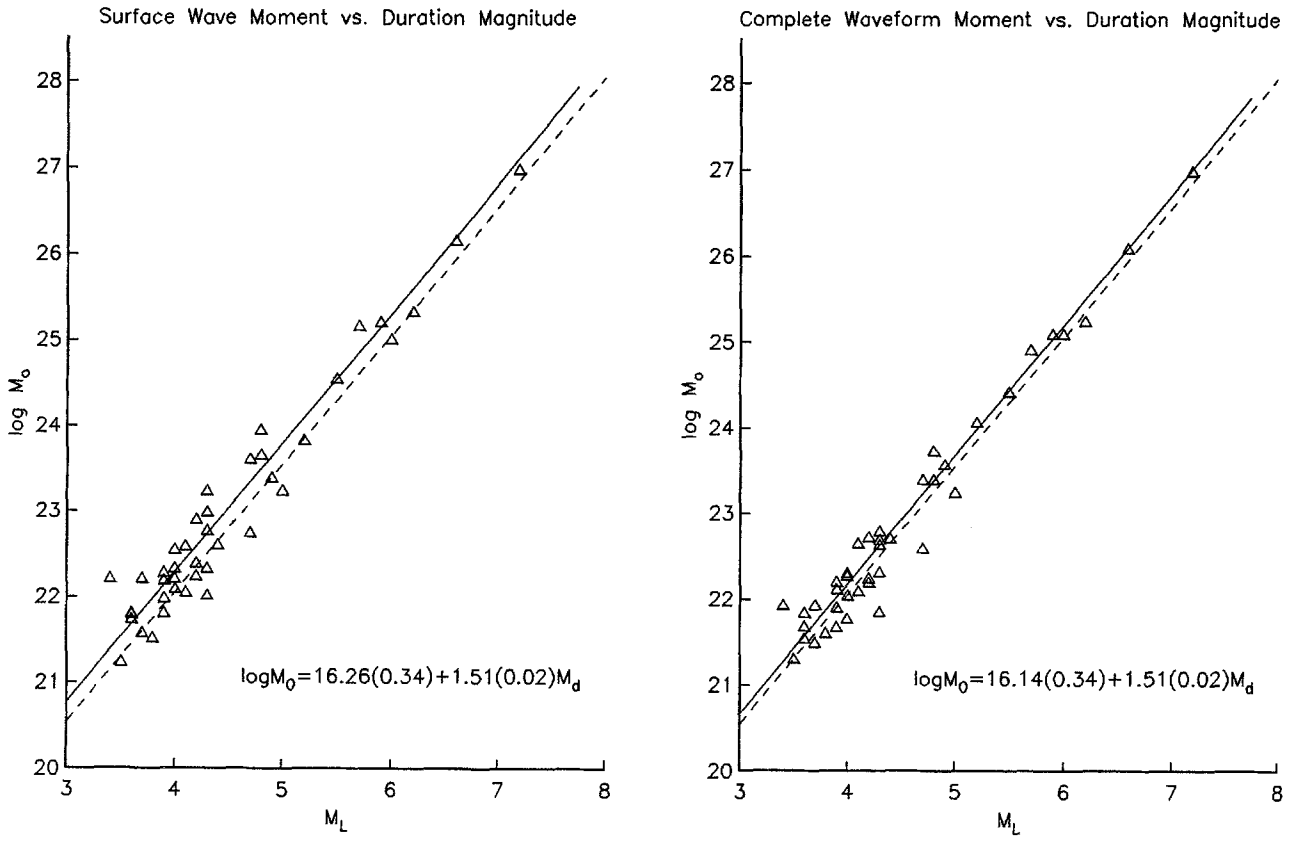

Figure 13. A comparison of M_0 and M_d for all events in the catalog. Otherwise, same as Figure 12.

plete waveform methods, respectively, and the differences between M_w and M_d are $+0.161 \pm 0.048$ and $+0.086 \pm 0.037$. In each case, the discrepancy between the individual moment-magnitude determinations (0.075) is in between each method's differences with the local and coda magnitudes, and the deviation on these measurements (± 0.011) is the least of any of these comparisons. The largest discrepancy that we find is a 0.213 difference between M_L and M_d.

Finally, a magnitude comparison is made between the regionally determined moment tensors and those determined teleseismically using the Harvard CMT technique (Dziewonski *et al.,* 1981). Figures 14 and 15 compare the results for M_w and the focal mechanism, respectively, between the final CMT and final regional surface-wave moment tensors. There are only a few CMT solutions reported for $M < 5.5$. As in the case of the two regional moment-tensor methods, the comparison of M_w is excellent, and there is practically no difference between the least-square regression and a straight one-to-one ratio, except for a slight difference over the extrapolated low-magnitude region. In addition, all of the moment-tensor comparisons plot below the 0.5 cutoff, with the exception of one magnitude 5 event, which falls at the lower threshold of routine CMT processing. In this particular case, the two regional methods are in agreement with each other. This is very encouraging in demonstrating that there is continuity between the global and regional moment-tensor inversions.

Quality Control of Automation Procedures

Of course, no automated system is completely foolproof. Noisy stations, imperfect models, and relying on computer locations can all contribute to produce incorrect moment-tensor solutions. As a result, procedures have been developed to try and prevent incorrect solutions from being broadcast. Parameters such as variance reduction, percent double couple, azimuthal aperture, number of stations, number of components, and depth resolution can all be factored in, determining the quality of the moment-tensor solution. By comparing the automatic moment-tensor solutions to the revised moment-tensor solutions in light of these parameters, we can optimize the quality function to determine whether or not we have a reliable solution. The current decision process mainly involves accepting or rejecting an automatic solution. In the future, this process will involve trying to incorporate more and more of the decisions of the analyst and trying to improve on the solution by taking a corrective course of action, such as adding or removing a given station from the data set.

Table 1
Statistical Differences in Magnitude Determinations

	M_w (RSW)	M_w (CWF)	M_L (BDSN)	M_d (NCSN)
M_w (RSW)	—	−0.075 ± 0.011	+0.053 ± 0.096	−0.161 ± 0.048
M_w (CWF)	+0.075 ± 0.011	—	+0.128 ± 0.079	−0.086 ± 0.037
M_L (BDSN)	−0.053 ± 0.096	−0.128 ± 0.079	—	−0.213 ± 0.057
M_d (NCSN)	+0.161 ± 0.048	+0.086 ± 0.037	+0.213 ± 0.057	—

Numbers shown are the mean and standard deviation of the difference of each column from each row. M_L and M_d values are obtaned from the Northern California Earthquake Data Center. There are 82 samples in each comparison.

Parameters of the moment-tensor solution are generated by an average of the parameters of the individual methods, weighted by the solution quality of the individual methods. For example, a very robust determination of M_w is computed as

$$M_w = \frac{(M_w^{(1)} * \mathrm{QUAL}^{(1)} + M_w^{(2)} * \mathrm{QUAL}^{(2)})}{\mathrm{QUAL}^{(1)} + \mathrm{QUAL}^{(2)}}, \quad (4)$$

where QUAL is the solution quality. Similar estimations can be made of other parameters, such as source depth.

In addition, the moment-tensor solutions can be compared to see if there are significant differences between the two mechanisms. Given that the methods often use different stations, different models, and different parts of the waveform, it is unlikely that both methods would generate the same incorrect solution. To date, there has only been one such event. The similarity of the two solutions can be used as a factor to assess the dependability of the moment-tensor solutions. We feel that, between the procedures to filter out bad data, the quality assessment of each method, and the comparison of the two methods, we can reliably generate automatic moment-tensor solutions in a timely manner.

We show several examples in order to illustrate how this works in practice. Figure 16 shows an example of automated moment tensors that were in close agreement with one another. The earthquake occurred on 1 December 1995 on the Hayward Fault north of Berkeley. The moment-tensor difference function ($\mu = 0.07$) was very close to zero. The seismic scalar moments vary quite a bit in this case ($M_0 = 4.8 \times 10^{21}$ and 1.7×10^{21} dyne-cm), differing in M_w by 0.3, but this is mainly caused by the different centroid depths determined by the automatic solutions by the two methods. Final solutions for this event are very similar to the automated moment tensors and yield M_w's of 3.7 and 3.6, which also compare favorably to the weighted average of $M_w = 3.6$, calculated using equation (4).

Figure 17 shows an example in which the methods were not in agreement. This event occurred on 5 December 1995 and was located beneath the Pacific Ocean along the Mendocino Fault at a distance of over 200 km west of Petrolia. In this case, the solutions look very different, and $\mu = 0.96$. Why were the two methods not in agreement? Due to the earthquake's location very far from shore, initial hypocenters of the event were highly inaccurate (differing more than 100 km in longitude from later readings that included S waves). The large mislocation prevented a quick and robust moment-tensor solution by either regional moment-tensor technique, and the solutions were in stark disagreement with each other. Clearly, in this case, the automatic solutions were different enough that they would not have passed any of the criteria for automatic broadcasting. The revised mechanisms using both moment-tensor methods indicate a right-lateral strike-slip earthquake on an east–west striking fault and M_w of 5.0. It is interesting to note that the average preliminary M_w estimate of 4.92 is very close to that of the revised solution.

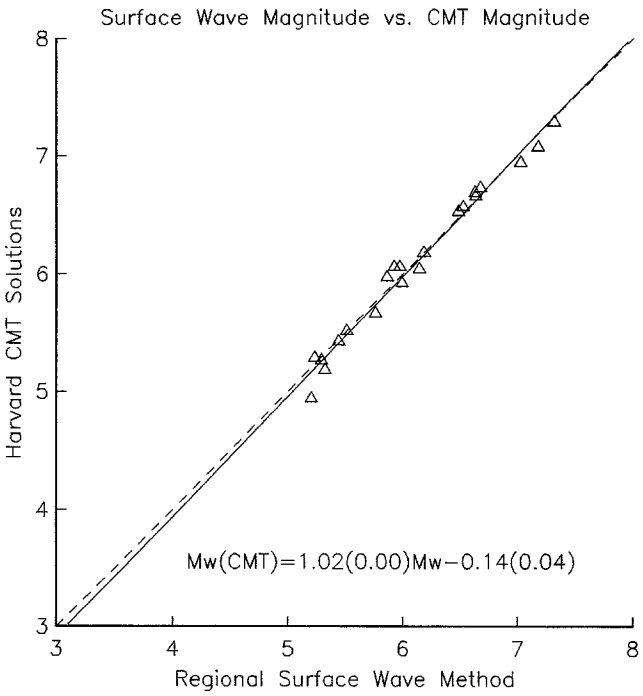

Figure 14. A comparison of two moment magnitudes, one from the regionally determined moment-tensor method and the other from Harvard CMT.

In the current configuration of the system with each moment-tensor procedure running independently, if the automatic solutions were immediately released, the moment-ten-

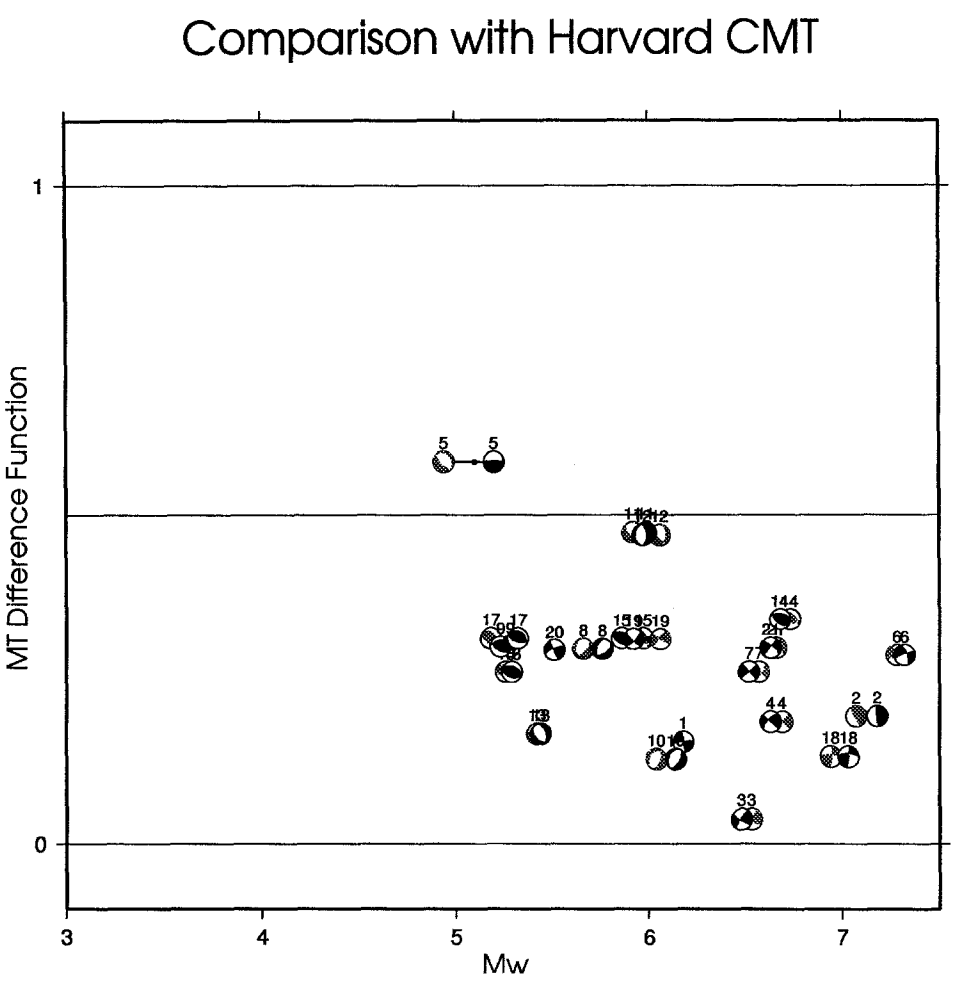

Figure 15. A comparison of the automatic regional surface-wave (gray) and Harvard CMT (black) moment-tensor solutions. Axes are the same as those in Figure 6. Numbers above the focal mechanisms are listed in chronological order.

sor solutions would generate reasonable solutions about 60% to 80% of the time and produce M_w within 0.1 magnitude units of the revised solutions about 50% to 70% of the time and within 0.2 magnitude units, about 80% to 90% of the time. These numbers are based purely on the previous performance of the system. By improving each of the independent methods and using the solutions from the two independent methods, we can generate the mechanism and magnitude reliably enough to immediately release, first moment magnitude, then complete moment-tensor solutions to the outside community.

Summary

Efforts have been made to streamline the two regional moment-tensor methods that are employed at the UC Berkeley Seismographic Station. The methods are fast and extremely effective at generating automatic moment tensors that are then human-reviewed and distributed to the outside community. Automating the regional moment-tensor methods have allowed us to generate reliable moment-tensor solutions for magnitude 3.5 earthquakes within 9 to 15 min of the occurrence of an event.

The current goal is to fully integrate these procedures into the REDI system. In the near future, locations will be produced more rapidly, and data will be available even earlier than in the current system (Gee *et al.*, 1996). These future advances in the methods used to telemeter and store the data can reduce the time necessary to generate the automatic moment-tensor solution to about 5 to 6 min, or about half of the current time, and is limited only by the time required for propagation of the seismic waves across the network.

Acknowledgments

This research was partially supported by USGS NEHRP Award Number 1434-93-G2311 and 1434-94-G2399 and is Contribution Number 96-4 of the U.C. Berkeley Seismographic Station.

Event Date/Time: 953352311

Data Used: Regional Surface Waves

Best Fitting Double-Couple:
Mo = 4.80E+21 Dyne-cm

Plane	Strike	Rake	Dip
NP1	51	-2	90
NP2	141	-180	88

Moment Magnitude = 3.75

Data Used: Complete Waveform Method

Best Fitting Double-Couple:
Mo = 1.70E+21 Dyne-cm

Plane	Strike	Rake	Dip
NP1	48	-7	88
NP2	138	-178	83

Moment Magnitude = 3.45

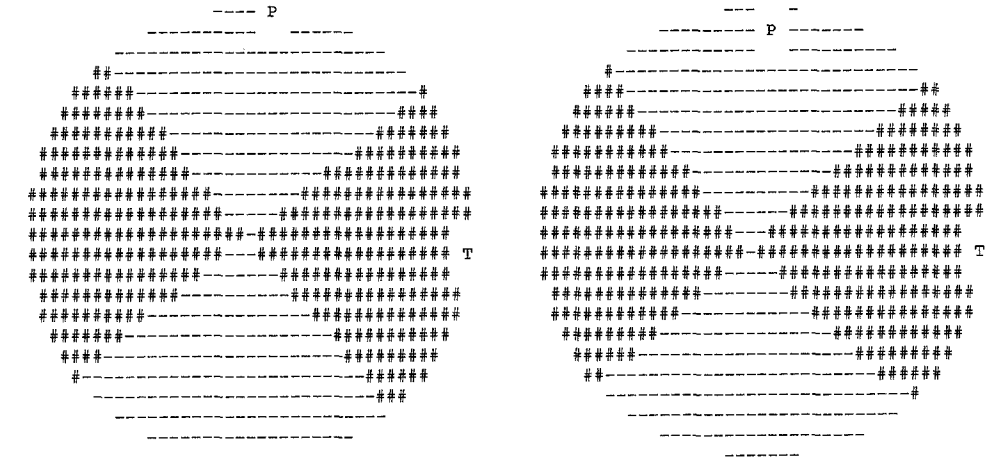

Figure 16. A comparison of automated solution for the 12/01/95 Berkeley event. Regional surface-wave solution shown on left, and complete waveform solution shown on right.

Event Date/Time: 953391928

Data Used: Regional Surface Waves

Best Fitting Double-Couple:
Mo = 5.40E+23 Dyne-cm

Plane	Strike	Rake	Dip
NP1	101	50	61
NP2	341	139	48

Moment Magnitude = 5.12

Data Used: Complete Waveform Method

Best Fitting Double-Couple:
Mo = 1.40E+23 Dyne-cm

Plane	Strike	Rake	Dip
NP1	106	-105	70
NP2	324	-55	25

Moment Magnitude = 4.73

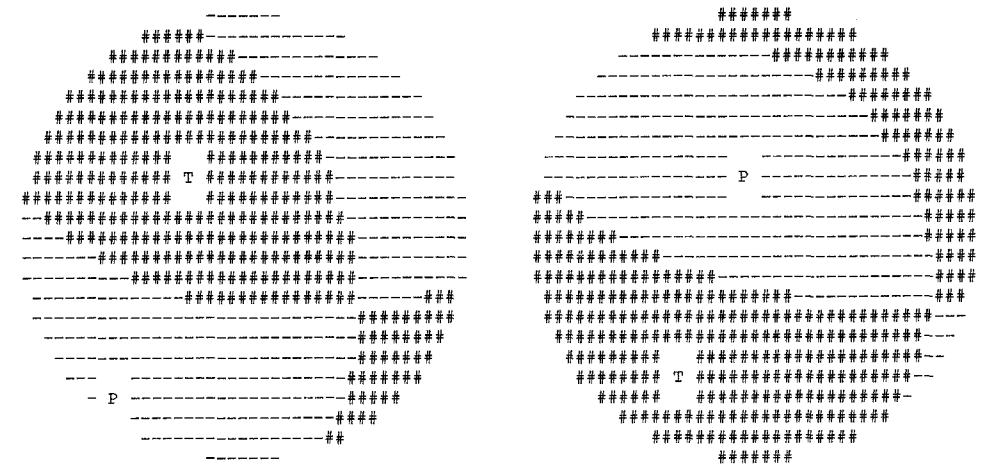

Figure 17. A comparison of automated solution for the 12/05/95 Mendocino Fault event. Regional surface-wave solution shown on left, and complete waveform solution shown on right.

```
This is a preliminary UCB moment tensor solution for
the 950618 22:23 UTC event located 21 km ESE of Quincy, CA
(39.84N; 120.72W; BDSN). The ML averaged across the BDSN
network was 4.4. A Mw 4.1 was obtained from long-period
three-component waves and surface wave amplitude and phase
spectra.

 Best Fitting Double-Couple

        Three-Component waves   Surface waves
    Mo = 1.52E+22 Dyne-cm       1.70e+22
    Mw = 4.1                    4.1
    Z  = 11km                   8 km
    NP1 = 212/-22/85            204/-32/68
    NP2 = 304/-175/68           307/-154/61


Regards,
Doug Dreger
Mike Pasyanos
UCB Seismographic Station

        Three-component waves solution
                   -------
              ------------------
            ----------------------##
          ------------------------######
        ---------------------------#########
      ####----------------------############
     ############-----------################
    ##################------##################
    ####################---###################
   ######################----###################
   ######################------##################
   ####################----------############
   #    ##############-------------##########
   # T ############-----------------########
      ############-------------------######
    ##############---------------------#####
     ############-----------------------###
      ##########-------------------------#
       ########--------------------------
         #####------------    ---------
           ##-------------- P -------
              ------------    ----
                   -------

     Lower Hemisphere Equiangle Projection
```

Figure 18. A typical moment-tensor E-mail. Shown for an M 4.1 earthquake near Quincy, California, that occurred on 18 May 1995.

References

Dreger, D. S. and D. V. Helmberger (1991). Complex faulting deduced from broadband modeling of the 28 February 1990 Upland earthquake (M_L = 5.2), *Bull. Seism. Soc. Am.* **81,** 1129–1144.

Dreger, D. S. and D. V. Helmberger (1993). Determination of source parameters at regional distances with single station or sparse network data, *J. Geophys. Res.* **98,** 8107–8125.

Dreger, D. and B. Romanowicz (1994). Source characteristics of events in the San Francisco Bay region, *U.S. Geol. Surv. Open-File Rept. 94-176,* 301–309.

Dreger, D., J. Ritsema, and M. Pasyanos (1995). Broadband analysis of the 21 September, 1993 Klamath Falls earthquake sequence, *Geophys. Res. Lett.* **22,** 997–1000.

Dziewonski, A. M., T. A. Chou, and J. H. Woodhouse (1981). Determination of earthquake source parameters from waveform data for studies of global and regional seismicity, *J. Geophys. Res.* **86,** 2825–2852.

Gee, L. S., D. S. Neuhauser, D. Dreger, M. Pasyanos, R. A. Uhrhammer, and B. Romanowicz (1996). Real-time seismology at UC Berkeley: the Rapid Earthquake Data Integration project, *Bull. Seism. Soc. Am.* **86,** 936–945.

Hanks, T. C. and H. Kanamori (1979). A moment magnitude scale, *J. Geophys. Res.* **84,** 2348–2350.

King, G., R. S. Stein, and J. Lin (1994). Static stress changes and the triggering of earthquakes, *Bull. Seism. Soc. Am.* **84,** 935–953.

Patton, H. and G. Zandt (1991). Seismic moment tensors of western U.S. earthquakes and implications for the tectonic stress field, *J. Geophys. Res.* **96,** 18245–18259.

Ritsema, J. and T. Lay (1993). Rapid source mechanism determination of large ($M_w \geq 5$) earthquakes in the western United States, *Geophys. Res. Lett.* **20,** 1611–1614.

Ritsema, J., T. Lay, D. Dreger, M. Pasyanos, and B. Romanowicz (1994). Moment tensor inversion for western United States earthquakes: calibration of methods, *Seism. Res. Lett.* **65,** 33.

Romanowicz, B. (1982). Moment tensor inversion of long-period rayleigh waves: a new approach, *J. Geophys. Res.* **87,** 5395–5407.

Romanowicz, B. and T. Monfret (1986). Source process times and depths of large earthquakes by moment tensor inversion of mantle wave data and the effect of lateral heterogeneity, *Ann. Geophys.* **74,** 271–283.

Romanowicz, B., L. Gee, and R. Uhrhammer (1992). Berkeley digital seismic network: a broadband network for northern and central California, *IRIS Newslett.* **XI,** 1–5.

Romanowicz, B., D. Dreger, M. Pasyanos, and R. Uhrhammer (1993). Monitoring of strain release in central and northern California using broadband data, *Geophys. Res. Lett.* **20,** 1643–1646.

Romanowicz, B., D. Neuhauser, B. Bogaert, and D. Oppenheimer (1994). Accessing northern California earthquake data via internet, *EOS* **75,** 258–261.

Thatcher, W. and T. Hanks (1973). Source parameters of southern California earthquakes, *J. Geophys. Res.* **78,** 8547–8576.

Thio, H. K. and H. Kanamori (1995). Moment tensor inversions for local earthquakes using surface waves recorded at TERRAscope, *Bull. Seism. Soc. Am.* **85,** 1021–1038.

Uhrhammer, R. A. (1986). Characteristics of northern and central California seismicity, *Bull. Seism. Soc. Am.* **57,** 21.

Appendix

Figure 18 illustrates a typical E-mail message that is sent out after an earthquake. We currently send out these moment-tensor messages to users at one of two requested status levels: either for all messages or for all events $M \geqq 4.5$. If you are interested in receiving these moment-tensor E-mails, please contact one of the authors.

Seismographic Station
Department of Geology and Geophysics
University of California, Berkeley
Berkeley, California 94720

Manuscript received 18 August 1995.